A novel structure of magnetic geared generator in dual-rotor wind turbine

Soheil Yousefnejad[1], Hossein Heydari[2], Vincenzo Cirimele[3], Jong-Suk Ro[4,5]

[1]Electrical Engineering Department, University of New Orleans, LA, USA
[2]Department of Electrical Engineering, Iran University of Science and Technology, Tehran, Iran
[3]Department of Electrical, Electronic, and Information Engineering, University of Bologna, Bologna, Italy
[4]School of Electrical and Electronics Engineering, Chung-Ang University, Seoul, South Korea
[5]Department of Intelligent Energy and Industry, Chung-Ang University, Seoul, South Korea

Article Info

ABSTRACT

Variable-speed constant-frequency generating systems are commonly employed in wind turbines to enhance efficiency and minimize losses. Additionally, the utilization of dual-rotor wind turbines enables the capture of a greater amount of wind energy, leading to a significant increase in efficiency. Traditionally, dual-rotor wind turbines are managed by a full-scale power converter, and the rotor current is transmitted through brushes, which substantially raises the system's cost. To address these challenges, this study introduces a novel configuration that enables power control with a smaller power converter. In contrast to conventional dual-rotor wind turbines that generate power using both rotors, the proposed structure designates one rotor as a system controller. Apart from these benefits, the proposed structure greatly enhances conversion performance by notably improving the power factor. A comparison with existing configurations described in literature is conducted to demonstrate the superiority of the proposed structure.
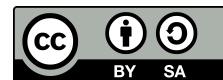
Corresponding Author:

Jong-Suk Ro
Department of Intelligent Energy and Industry, Chung-Ang University
Seoul, South Korea
Email: jongsukro@gmail.com

NOMENCLATURE

η	efficiency of the motor
A_1	electric loading of inner airgap
A_2	electric loading of the outer airgap
a_m	magnitude of the magneto motive force
a_n	magnitude of the permeance
$B\theta_{in}$	tangential components of the magnetic flux density in the inner airgap
$B\theta_{out}$	tangential components of the magnetic flux density in the outer airgap

B_{g1} loading of magnetic

B_{g2} magnetic loading

Br_{in} radial components of the magnetic flux density in the inner airgap

Br_{out} radial components of the magnetic flux density in the outer airgap

D_{l1} outer diameter of the inner stator

D_{l2} outer diameter of the outer stator

I_{ph1} current of the inner stator

I_{ph2} current of the outer stator windings

K_w fundamental winding factor

L_{stack} length along the axial direction

N_{ri} number of pole pairs of the inner rotor

N_{ro} number of pole pairs of the outer rotor

N_{ts1} inner winding series turns

N_{ts2} outer winding series turns

P_0 permeance of the steel pole pieces

P_{osi} power of the inner stator

P_{oso} power of the outer stator

P_{si} number of pole pairs of the inner stator

R_{in} radius of the inner stator

R_{out} radius of the outer stator

W_{ro} speed of the outer rotor

1. INTRODUCTION

The growing demand for electric energy and rising environmental concerns have led to a continuous surge in the interest surrounding wind energy as a source of electricity production. Currently, there are four distinct configurations that are commonly employed to manage the electric energy from wind power. These configurations are outlined [1], [2]: constant speed squirrel-cage induction generator [3], doubly fed induction generator [4], brushless generator with gear and full converter (GFC), and direct-drive generator system.

With respect to other counterparts, the direct-drive generator system configuration operates in absence of a gearbox [5]–[8]. This forces to increase the number of poles of the generator in order to efficiently operate at low speed [9]. Hence, despite such a gearless generator system needs less maintenance and owns higher reliability than the geared counterpart, the gearless generator is bulkier and heavier. Therefore, a gearless generator system requires heavier and larger nacelle for the turbine so which increases the cost of the tower and limits the use of gearless generator systems in current industry. Furthermore, this configuration reveals less torque density with respect to high-speed generators. Consequently, the use of gearboxes has remained widely adopted in wind turbines. On the other hand, an economic analysis conducted on the turbine in the wind generators, reveals that the significant cost of the whole price of the turbine is related to the gearbox. In addition to its relevant cost, the gearbox introduces several issues related to fault tolerance and maintenance. All the summarized aspects, underlines that research on the gearbox is still important and necessary [10]. The most recent research in this field is putting in evidence the possibility to substitute the mechanical gear with a

contactless version [11]. This contactless gear transfers torque between the rotating parts by taking advantage of the interactions of arrays of permanent magnets (PMs). This is why this kind of gears is typically called magnetic gear [12]. Through the evolution of magnetic gears, an arrangement based on the integration of generator and magnetic gear is presented in [13], [14]. This structure aims to decrease both size and price of the ensemble of gear and generator [15]. The mentioned arrangement consists of a dual-rotor and a double stator [16]. So, the resulting electrical machine is divided into two sections consisting of: i) inner stator windings and inner rotor and outer rotor performing as a magnetic-geared permanent magnet machine (MGPM machine) where the magnetic gear's rotor is substituted by stator windings [17], and ii) outer rotor and outer stator windings performing as a synchronous machine.

A similar structure has been proposed for vehicle powertrains as it allows to control the wheel's speed without rigid constraint with respect to the speed of the internal combustion engine with a consequent increase in efficiency and decrease of fuel consumption [17], [18]. As shown in Figure 1, the proposed structure can be inserted in the wind turbine structure where the inner rotor of the proposed structure is connected to the main wind turbine rotor and the outer rotor is connected to an auxiliary wind turbine rotor. In this configuration, the proposed structure can increase the input power of the wind turbine by using two wind rotors. In other words, the auxiliary rotor can act as an additional power source for the system. In the studies [19]–[25], there are different structures in which both rotors power the system. Differently from the latter, in the structure proposed in this work, the inner rotor acts as power input for the system while the outer rotor is used both as power input and as system controller through the interaction with the outer stator windings [26]. The auxiliary rotor subsequently causes a need for the power electronic converter with nominal power less than the nominal power of the wind turbine. Thus, in the proposed configuration, the nominal power of the power electronic converter can be lower than the nominal output power of the wind turbine as the outer rotor provides the power needed to control the whole output power of the system. Therefore, compared to the counterparts mentioned above, this configuration requires a less expensive converter. Moreover, the output power is produced at a constant frequency since the outer stator can control the system. Therefore, the full-scale power converter for output power is eliminated. In addition to these advantages, a novel structure is here considered for the magnetic gear which allows to improve the electro-mechanical performances by reducing torque ripple and harmonic component in the output voltage. Moreover, some studies proposed various structures with the aim of enhancing the machine's performance such interior permanent magnet which magnets inserted inside the rotor core [27] and dual-layer PM excitation and Halbach PM array [28]–[31]. The structure proposed in this work moves from the results of these previous works introducing a structure that merged the dual-layer PM excitation and the Halbach PM array aimed at increasing the power factor of the whole machine.
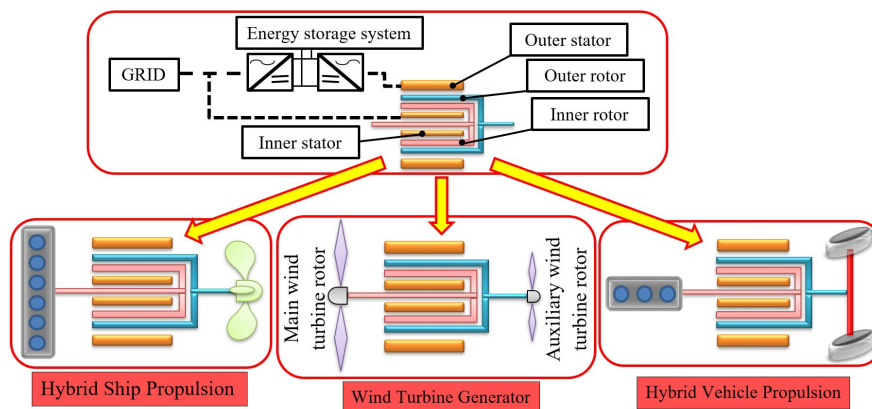

Figure 1. Possible integrations of the proposed structure, which can be used in wind turbines as well as in hybrid electric vehicle (HEV and ship propulsion)

Hence, in short, the structure proposed in this work has four advantages. i) It requires less maintenance due to eliminating the mechanical gearbox in the wind turbine system [32]. ii) It requires a smaller power converter compared to other traditional gearless generator systems, and this leads to a decrease in the system cost [33]. iii) It can be advantageously integrated with a dual-rotor wind turbine which is more efficient than a conventional single-rotor one. iv) It owns a higher power factor than the former magnetic geared generator, by

combining some structures [6], [16].

The aim of this paper is to present and analyze the mentioned novel structure of permanent magnet magnetic gear combined with a synchronous machine based on the combination of the two topologies of the dual-layer PM excitations and the Halbach PMs array. The structure of PMs magnetic gear integrated with the synchronous machine is referred to as magnetic geared generator (MGG). This paper is structured as follows: section 2 presents the configurations of both the proposed and conventional structures, along with an explanation of the corresponding magnetic flux distributions. Moving on to section 3, a comprehensive flowchart of the proposed structure's design is provided, encompassing all design steps and parameters. In section 4, a comparative assessment of the magnetic fields of the structures is presented. Following that, section 5 undertakes a comparison of the flux, voltage, and torque characteristics exhibited by these structures. Section 6 exclusively examines the variable-speed constant-frequency performance demonstrated by the proposed structure.

2. GENERAL TOPOLOGY OF NOVEL STRUCTURE OF MGG

The novelty of the MGPM's proposed structure rests on two key principles, as: i) the dual-rotor wind turbine employs one of its rotors as a system controller and ii) by combining two distinct structures, the proposed design significantly enhances power quality while reducing torque ripple. These two crucial aspects, representing the primary innovations of this study, are thoroughly elaborated upon in this section.

2.1. Dual-rotor wind turbine in the proposed configuration

The inner stator produces output power toward the grid and the outer stator controls the proposed structure but both the main and auxiliary wind turbine rotors capture the energy from the wind. The inner and outer rotor and inner stator act as an MGPM machine and the outer rotor and outer stator act as a synchronous machine. Then, the outer stator can control the outer rotor speed and the inner stator can be handled with the inner and outer rotor. In order to control the output power of the inner stator, the outer stator is controlled by a converter. Furthermore, the outer rotor speed supplies the auxiliary power for the system leading to a smaller power converter for the outer stator.

2.2. Integration of two structures in the proposed structure

Typically, magnetic gears are commonly associated with a significant limitation: comparatively modest torque density [34]. To enhance the performance indicator mentioned above, one possible avenue for improvement is the utilization of a Halbach PM array along with dual-layer PM excitation [28, 35]. This study aims to integrate these structures, leveraging the respective advantages of both. The Halbach PMs array refers to a specific configuration of PMs that enables the creation of a unique spatial magnetization pattern. This arrangement facilitates the amplification of magnetic flux on a desired side, while simultaneously reducing it on an undesired side (i.e., a not convenient from the power conversion point of view). As discussed in references [36]–[38], by implementing the Halbach structure, a substantial improvement in torque density and a significant reduction in torque ripple can be achieved. Figure 2 illustrates an example application of this concept, demonstrating the configuration of PM and steel poles. This configuration is discussed in [30] and [39] and the focus of this design is to enhance torque output. In this configuration, all PMs in both rotors are magnetized in the same direction, and they are positioned adjacent to steel pole pieces, creating a specific alternating pattern of PMs and steel pole pieces. This sequence is maintained in both the inner and outer rotors. As a result, both rotors generate and control the magnetic field concurrently. This arrangement is typically referred to as "bi-directional flux modulating" [40] while the related structure is referred to as "dual-layer magnetic geared generator (DL-MGG)". As discussed in [40], the proposed design exhibits greater torque output than conventional structures, despite having a higher torque ripple. The concentration of the magnetic field distribution is illustrated in Figure 3 .

The novel structure proposed here is referred to as "Halbach dual-layer magnetic geared generator (HDL-MGG)" and whole electric machine whose configuration is sketched in Figure 4 and its arrangement is shown in Figure 5 Despite the strong similarity with respect to the DL-MGG structure, the proposed HDL-MGG owns a different direction magnetization of the PMs. The magnetization directions of the PMs in the DL-MGG structure are arranged according to a Halbach PM array. This arrangement aims to amplify the magnetic flux in the air gaps while minimizing it in other regions. As a result, this configuration leads to an

augmentation in torque, a reduction in torque ripple, and an improvement in power factor. The characteristics of the magnetic flux distribution in the different airgaps of the HDL-MGG are described in 2.2.1. to 2.2.3.
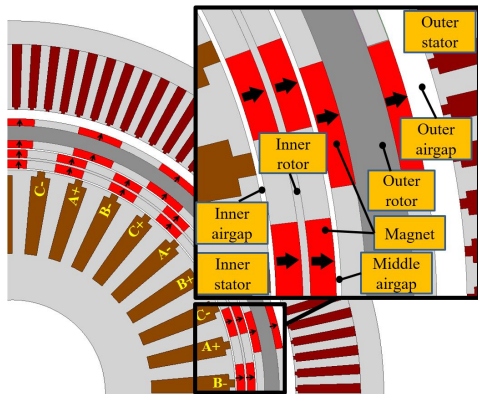

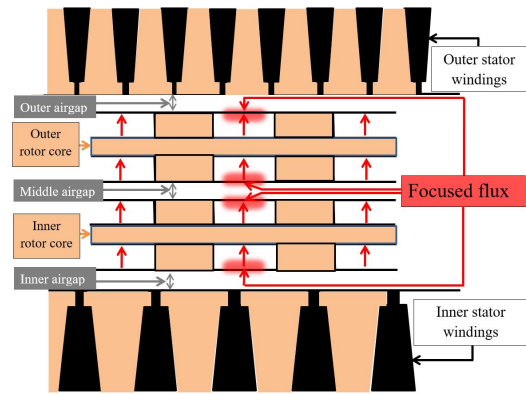Figure 2. Dual-layer magnetic geared generator (DL-MGG) structure

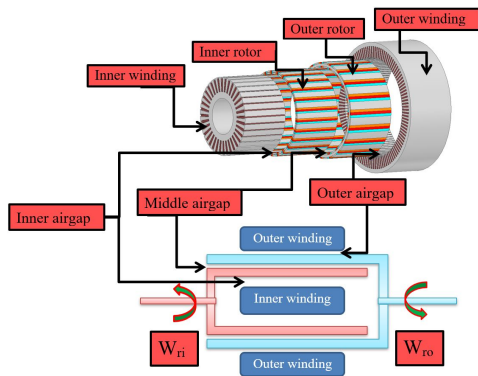Figure 3. Concentration of the magnetic fluxes in the DL-MGG

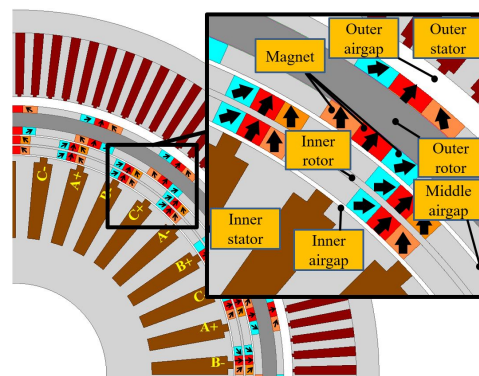Figure 4. Whole configuration of the proposed HDL-MGG structure

Figure 5. Structure of the Halbach dual-layer magnetic geared generator (HDL-MGG)

2.2.1. Outer airgap

The magnetic flux distribution in the outer airgap can be seen as the combined effect of three main flux components: i) flux created by the excitation of the outer windings, ii) flux associated with the outer rotor PMs, and iii) flux modulated by the outer rotor steel pole pieces. By employing the Halbach PMs array arrangement, shown in Figure 6, the magnetization directions of the outer rotor PMs are concentrated, resulting in an augmentation of the magnetic fluxes in the outer air gap. This magnetic field amplification contributes to a higher torque density and improved power factor.
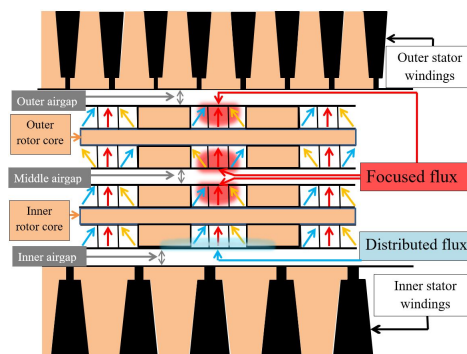

Figure 6. Concentration of the magnetic fluxes in the HDL-MGG

2.2.2. Middle airgap

The magnetic flux distribution in the middle air gap is influenced by four key components. These components include i) the flux that is modulated by the steel pole pieces of the inner rotor, ii) the flux that is modulated by the steel pole pieces of the outer rotor, iii) the flux associated with the PMs in the inner rotor, and iv) the flux associated with the PMs in the outer rotor. In summary, both inner and outer rotors modulate the magnetic field via steel pole pieces and create a magnetic field through the PMs inserted in the rotors (i.e., the mentioned bi-directional flux modulation).

2.2.3. Inner airgap

The magnetic flux distribution in the inner airgap can be seen as the combined effect of three main flux components: i) flux modulated by the inner rotor steel pole pieces, ii) flux associated with the inner rotor PMs, and iii) flux is created by the excitation of the inner windings. As shown in Figure 6, in the inner airgap, only the magnetic flux created by the inner rotor PMs adjacent to the inner airgap is lowered. This decreases the harmonic distortion and torque ripple and increases the power factor. In this work, the Halbach dual-layer magnetic geared generator type2 (HDL-MGG type2) is proposed which is shown in Figures 7 and 8. This structure, despite the HDL-MGG augments whole the magnetic fluxes in all the airgaps. In order to show the effect of the flux density in the airgaps and show the introduced benefits, the HDL-MGG is compared with HDL-MGG type2. It is expected that the torque ripple of HDL-MGG type 2 is higher than HDL-MGG.
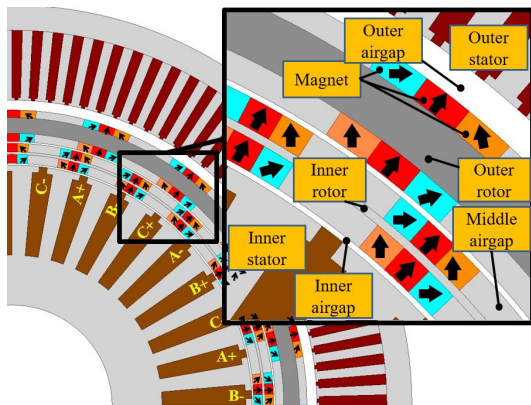

Figure 7. Structure of the Halbach dual-layer magnetic geared generator type2 (HDL-MGG type2) structure
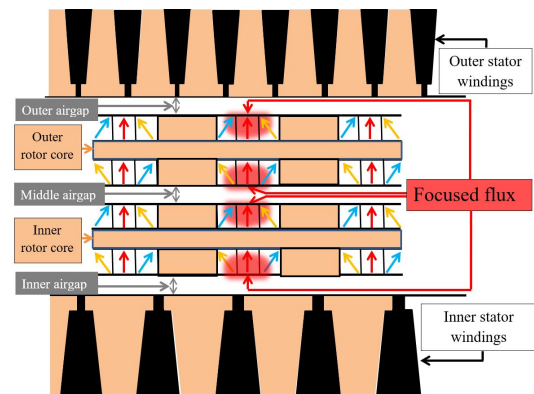

Figure 8. Concentration of the magnetic fluxes in the HDL-MGG type 2

3.   PRINCIPLE OF OPERATION AND DESIGN PARAMETERS

The design flowchart of the proposed structure (HDL-MGG) is shown in Figure 9. In step 1, in order to show the superiority of the proposed structure over other counterparts, a comparison is implemented in which the following design parameters are assumed constant: the product D^2L (where D is the overall radius of 160 mm and L is the stack length equal to 120 mm) and the PM volumes of 0.0053 m^3.

In step 2, there are some options to select the type of silicon steels for motor cores like M43, M27, and M19, with increasing M numbers corresponding to higher core losses but lower material costs. In this study, a cost-oriented approach was adopted to minimize expenses. Therefore, M43 steel was chosen for the stator core, stator teeth, and rotor teeth, while aluminum was selected for the rotor core.

Step 3 is divided into two sub-steps, focusing on the designs of the inner and outer rotors, respectively. In step 3-1, the first sub-step involves examining the relationship between the speeds of the rotors, the magnetic fields, and the torque of the inner rotor. The Fourier series representations of the permeance distribution P(θ) and the magneto motive force F(θ) are provided for the inner and outer rotors, as well as the inner stator [41].

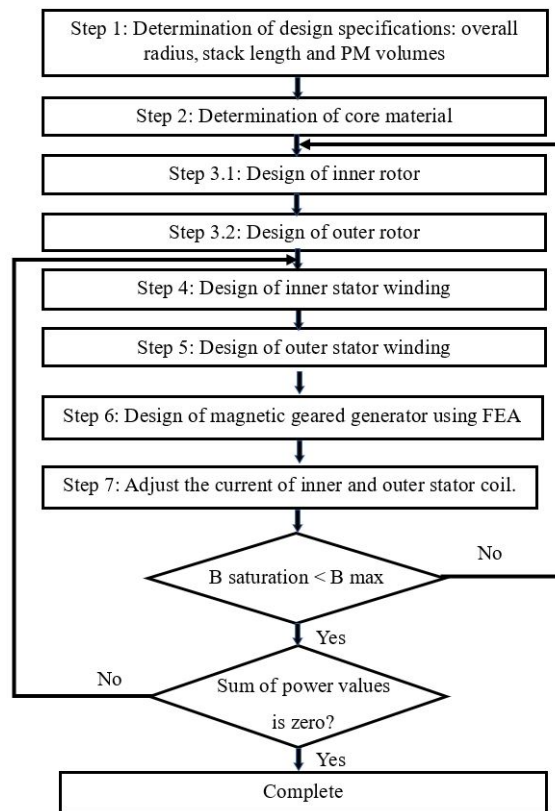$$P(\theta) = P_0 + \sum_{n=1}^{\infty} a_n sin((2n-1)N_{ri}\theta) \tag{1}$$

Figure 9. Design flowchart of the proposed structure

$$F(\theta) = \sum_{m=1}^{\infty} a_m sin((2m-1)P_{si}\theta) \qquad (2)$$

Then, the magnetic flux distribution of the proposed structure is expressed by (3) [41]:

$$\phi(\theta) = F(\theta).P(\theta) \qquad (3)$$

$$\phi(\theta) = P_0 \sum_{m=1}^{\infty} a_m sin((2m-1)P_{si}\theta) + \sum_{m=1}^{\infty}\sum_{n=1}^{\infty} \frac{a_m a_n}{2}$$
$$cos((2n-1)N_{ri} - (2m-1)P_{si})\theta) - cos((2n-1)N_{ri} + (2m-1)P_{si})\theta) \quad (4)$$

where H_1, H_2, H_3 and H_4 are the harmonic component of the magnetic flux, as (5) to (11).

$$H_1(m) = (2m-1)P_{si} \qquad (5)$$

$$H_2(n) = (2n-1)N_{ri} \qquad (6)$$

$$H_3(m,n) = (2n-1)N_{ri} - (2m-1)P_{si} \qquad (7)$$

$$H_4(m,n) = (2n-1)N_{ri} + (2m-1)P_{si} \qquad (8)$$

$$\phi(\theta) = F_{\Delta t}(\theta).P_{\Delta t}(\theta) \qquad (9)$$

$$\phi(\theta) = F(\theta - W_{si}\Delta t).P(\theta - W_{ri}\Delta t) \qquad (10)$$

$$\phi(\theta) = \sum_{m=1}^{\infty} P_\theta a_m sin(H_1(m)(\theta - W_{si}\Delta t)) \sum_{m=1}^{\infty} \sum_{n=1}^{\infty} \frac{(a_m a_n)}{2}$$
$$cos(H_3(m,n)(\theta - \frac{H_1(m)W_{ri} - H_2(m)W_{si}}{H_3(m,n)}\Delta t) - cos(H_4(m,n)(\theta - \frac{H_1(m)W_{ri} - H_2(m)W_{si}}{H_4(m,n)}\Delta t) \qquad (11)$$

The angular velocity of $H_1(m)$ is denoted as W_{si}, which represents the rotational speed of the magnetic fields of the inner stator. On the other hand, W_{ri} signifies the rotational speed of the inner rotor [41]. Subsequently, it is necessary for the number of pole pairs of the inner stator or outer rotor to be equal to $H_3(m,n)$ and $H_4(m,n)$, respectively. Furthermore, the relationships between the number of pole pairs must satisfy the specified condition [42]:

$$N_{ro} = N_{ri} - P_{si} \qquad (12)$$

The connections between the angular velocities is expressed by (13) [40] :

$$-N_{ri}w_{ri} + N_{ro}w_{ro} + p_{si}w_{si} = 0 \qquad (13)$$

Finally, the inner rotor torque can be expressed as (14):

$$T_{inner} = (\frac{L_{stack}R_{in}^2}{\mu_0}) \int_0^{2\pi} B_{rin}B_{in} \, d\theta \qquad (14)$$

In step 3-2, in addition to the inner rotor, the outer rotor is also composed of PM and steel pole piece sequences. As a result, the torque exerted by the outer rotor can be expressed in a similar manner:

$$T_{outer} = (\frac{L_{stack}R_{out}^2}{\mu_0}) \int_0^{2\pi} B_{rout}B_{out} \, d\theta \qquad (15)$$

In step 4, the inner stator in this structure acts like the inner rotor in conventional magnetic gear. The rotational speed of the magnetic field produced by the inner stator is expressed as:

$$w_{si} = \frac{(N_{ri}w_{ri} - N_{ro}w_{ro})}{(N_{ri} - N_{ro})} = \frac{(N_{ri}w_{ri} - N_{ro}w_{ro})}{p_{si}} \qquad (16)$$

Subsequently, the correlation between the frequency of the inner stator and the velocities of the inner and outer rotors is represented as:

$$f_{si} = \frac{(N_{ri}w_{ri} - N_{ro}w_{ro})}{60} \qquad (17)$$

In step 5, the outer stator and outer rotor function together as a synchronous machine. To achieve maximum torque output, it is essential for the number of poles in the outer stator and outer rotor to be identical. Moreover, the connection between the frequency and the number of pole pairs in the outer stator can be described by (18):

$$f_{so} = \frac{(p_{si}w_{si})}{60} \qquad (18)$$

In step 6, the MGPM generators are simulated using Ansys, a software based on the finite element method. The purpose of this simulation is to compare these machines and illustrate their respective advantages and disadvantages. In step 7, in the proposed machine, the inner stator torque in the inner airgap is expressed as in (19).

$$T_{si} = \frac{\pi}{2\sqrt{2}}\eta K_w A_1 B_{g1} D_{l1}^2 L_{stack} \tag{19}$$

$$A_1 = (6/(\pi D_{l1}))N_{ts1}I_{ph1} \tag{20}$$

In step 7, in the proposed machine, the inner stator torque in the inner airgap is expressed as (21) and (22) [41].

$$T_{so} = \frac{\pi}{2\sqrt{2}}\eta K_w A_2 B_{g2} D_{l2}^2 L_{stack} \tag{21}$$

$$A_2 = (6/(\pi D_{l2}))N_{ts2}I_{ph2} \tag{22}$$

It should be noted that the structures should not be saturated and also by considering adhering to the principle of energy conservation and assuming no power losses and the total power of the system should be zero as (23) [42].

$$P_{osi} + T_{inner}W_{ri} + T_{outer}w_{ro} + P_{oso} = 0 \tag{23}$$

3.1. Design parameter

To evaluate the superior performance of the proposed structure, a comparison is conducted with the previously discussed counterparts. This comparison is based on the assumption of identical overall radius, axial length, as well as PMs and copper volumes for all the machines under analysis. The key parameters of the Magnetic Geared Generators being analyzed are provided in Table 1.

Table 1. Design parameters

Parameter	Value
Stack length	120 mm
Overall radius	160 mm
Internal radius of outer stator	122 mm
Outer radius of the outer rotor	118 mm
Inner radius of the outer rotor	105.4 mm
Outer radius of the inner rotor	104.7 mm
Internal radius of inner rotor	96.7 mm
Outer radius of the inner stator	96 mm
Internal radius of inner stator	40 mm
Outer rotor permanent magnet thickness adjacent to outer air gap	3.02 mm
Thickness of the permanent magnet of the outer rotor adjacent to the middle air gap	3.29 mm
Thickness of the PMs of the inner rotor adjacent to the middle air gap	3.42 mm
Thickness of the PMs of the inner rotor adjacent to the inner air gap	3.57 mm
Number of pole pairs of internal stator coil	6
Number of pole pairs of outer stator coil	19
Number of pole pairs of inner rotor PM	25
Number of pole pairs of outer rotor PM	19
Number of internal stator slots	36
Number of outer stator slots	114
Number of phase	3
Number of internal stator coil conductors	25
Number of outer stator coil conductors	25
Magnet flux density (NdFeB)	1.1 T
Magnet relative permittivity	1.0446
PMs volume	0.0053 m^3
Stator core material	M43-29G

4. MAGNETIC FIELDS HARMONIC ANALYSIS

4.1. Inner airgap flux density excited by the inner rotor PMs

Figure 10(a) displays the harmonic spectrum of the radial flux density in the inner airgap, which is excited by the inner rotor's PMs. As depicted in the figure, the proposed HDL-MGG exhibits the lowest magnitude for the 25th harmonic in the flux density distribution. Conversely, the HDL-MGG type2 structure demonstrates the highest magnitude for this particular harmonic due to the influence of the Halbach PMs array in the system. This significant reduction of the 25th harmonic in the proposed structure is advantageous since it

does not contribute significantly to torque production in the machine. Furthermore, the fundamental harmonic component in these machines within the inner airgap is the 6th harmonic. In the proposed structure, the 6th harmonic possesses the highest magnitude, whereas it is the lowest in the DL-MGG structure. However, the amplitude of the 19th harmonic of the magnetic flux is enhanced thanks to the adoption of the Halbach PMs array in both inner and outer rotor PMs.

4.2. Inner airgap flux density excited by the outer rotor PMs

The harmonic frequency spectrum of the flux density in the inner airgap, which is induced by the outer rotor PMs, is depicted in Figure 10(b). As illustrated in the figure, the waveforms of HDL-MGG and HDL-MGG type 2 are identical since the magnetization directions of the outer rotor PMs are the same. It can be observed that the harmonic content in the proposed structure is equivalent to that of the HDL-MGG type 2 structure, and both structures exhibit higher harmonic content compared to the DL-MGG structure. In the proposed HDL-MGG structure, the amplitude of the primary harmonics of the magnetic flux in the outer airgap is increased due to the enhancement of the magnetic fluxes induced by the outer rotor PMs.
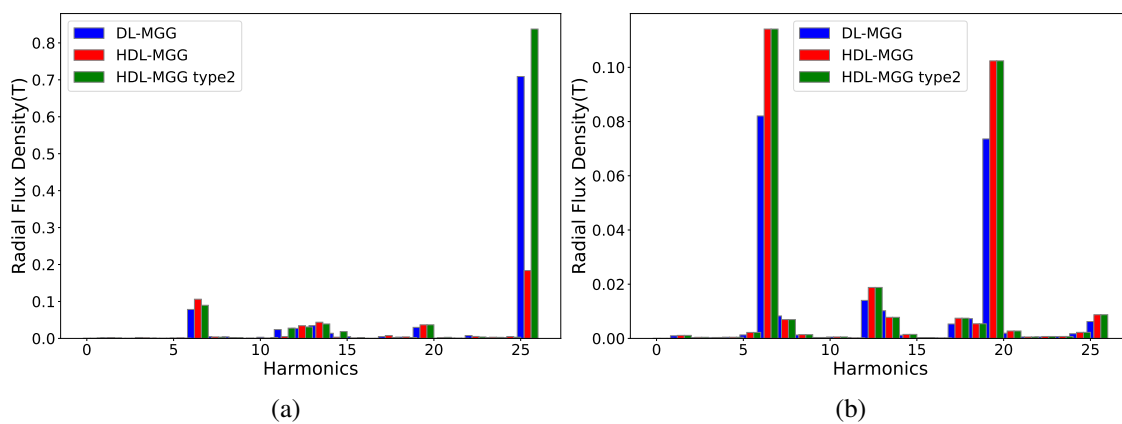

Figure 10. Harmonic spectrum of the inner airgap flux density excited by (a) the inner and (b) outer rotor PMs

4.3. Middle air gap flux density excited by the inner rotor PMs

Figure 11(a) illustrates the spatial harmonic frequency spectrum of the radial flux density in the middle airgap, which is excited by the inner rotor PMs. In the middle airgap, the fundamental harmonics of the magnetic flux are the 19th and 25th harmonics, attributed to the bidirectional flux modulation effect. Interestingly, in the proposed HDL-MGG structure, the 25th harmonic of the magnetic flux is the highest among all harmonic orders, whereas in the DL-MGG structure, it is the lowest. This implies that the proposed structure exhibits a higher torque output compared to the other configurations.
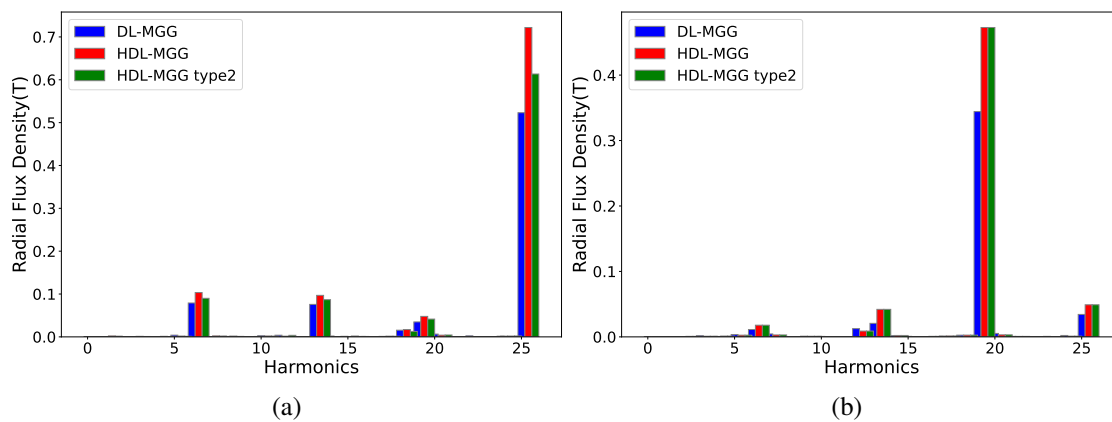

Figure 11. Harmonic spectrum of the middle air gap flux density excited by (a) the inner and (b) the outer rotor PMs

4.4. Middle air gap flux density excited by the outer rotor PMs

As depicted in Figure 11(b), the amplitude of the 19th harmonic of the magnetic flux induced by the outer rotor PMs in the middle airgap is higher than that of other harmonic components. This indicates that the proposed structure has the ability to generate a higher torque density compared to the DL-MGG structure. Additionally, the waveforms of the flux density in both the HDL-MGG and HDL-MGG type 2 structures are identical since the magnetization directions of the outer rotor PMs are the same.

4.5. Outer air gap flux density excited by the outer rotor PMs

As depicted in Figure 12, the 19th harmonic component stands out as the primary harmonic in the outer airgap. Moreover, the harmonic spectrum of the flux density in both the HDL-MGG and HDL-MGG type 2 structures is identical, as the magnetization directions of the outer rotor PMs are the same. Furthermore, the proposed structures (HDL-MGG and HDL-MGG type 2) exhibit higher torque density compared to the DL-MGG structure. This is attributed to the presence of a higher 19th harmonic component in the flux density generated by the proposed structures.
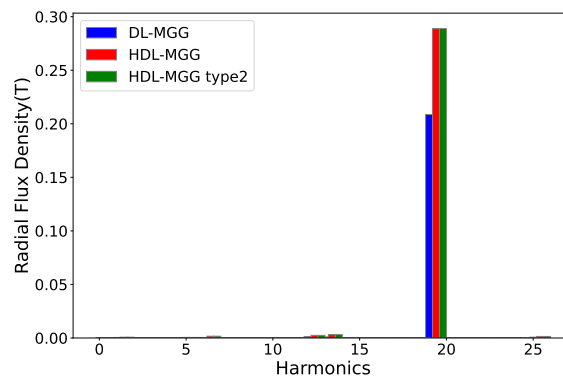

Figure 12. Harmonic spectrum of the outer air gap flux density excited by the outer rotor PMs

4.6. Air gaps flux density excited by the outer winding excitation

As depicted in Figure 13(a), the magnitude of the 19th harmonic in the magnetic flux induced by the outer winding excitation in the outer airgap is significantly higher compared to other harmonics. This indicates that the 19th harmonic plays a prominent role as the primary harmonic in the outer airgap when considering the outer winding excitation.
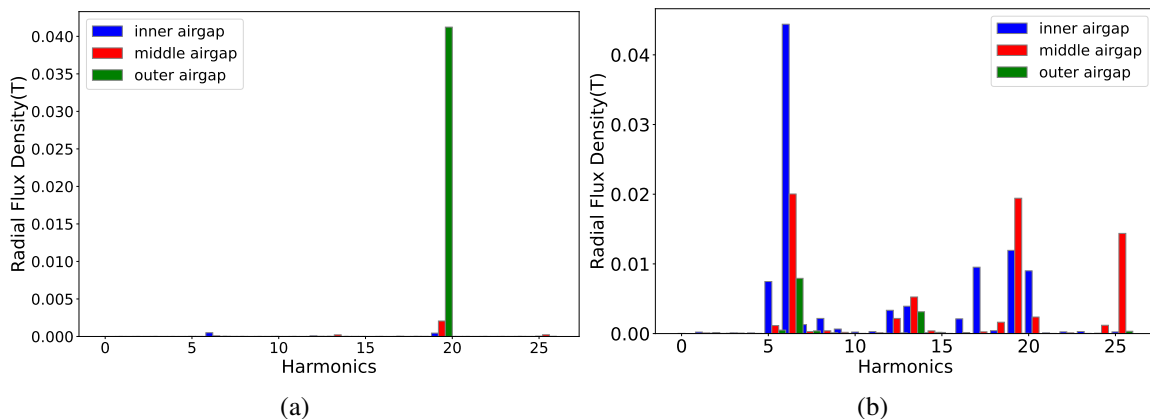

(a)

(b)

Figure 13. Harmonic spectrum of the air gaps flux density excited by (a) the outer and (b) the inner stator excitation

4.7. Air gaps flux density excited by the inner winding excitation

As depicted in Figure 13(b), In the inner airgap, the amplitude of the 6th harmonic in the magnetic flux induced by the inner winding excitation is notably high, indicating its significance as the primary harmonic in

this airgap. Additionally, it can be observed that the 25th harmonic component does not exert a significant impact in the inner airgap. In the proposed HDL-MGG structure, this particular harmonic component is attenuated by the implementation of the Halbach array, resulting in its reduced influence.

5.   COMPARISON OF DESIGNS

As depicted in Figure 14, the flux linkage of the proposed structure surpasses that of other counterparts. Moreover, the waveforms of the flux linkage exhibit a close resemblance to sinusoidal patterns. As it is demonstrated in Figure 15(a), the waveform of the no-load back-electromotive force (back-EMF) closely resembles a sinusoidal pattern. Notably, the back-EMF of the HDL-MGG structure exceeds that of the other structures. Additionally, as illustrated in Figure 15(b), the back-EMF voltage of the outer stator in the HDL-MGG structure is higher than in the other structures. The waveforms of both the HDL-MGG and HDL-MGG type 2 structures are identical due to the same magnetization directions of the PMs. Furthermore, in the proposed structure, the distribution of the magneto-motive force in the airgaps closely resembles a sinusoidal pattern, indicating a desired reduction in torque ripple. In this case, all waveforms exhibit sinusoidal characteristics. However, according to Table 2, it is evident that the proposed HDL-MGG structure exhibits the highest power factor, while the DL-MGG structure demonstrates the lowest power factor. Figure 16 shows the torque of the structures versus current. As it is shown, the torque of the machine is increased till the knee point and after that the torque rate is decreased. thus, the auxiliary rotor can be controlled well before 9 A/mm^2.
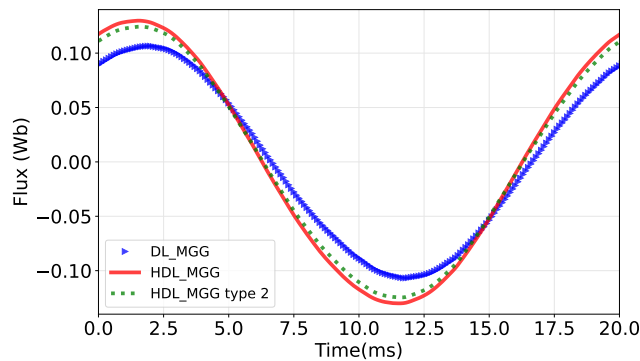

Figure 14. Flux linkage waveforms

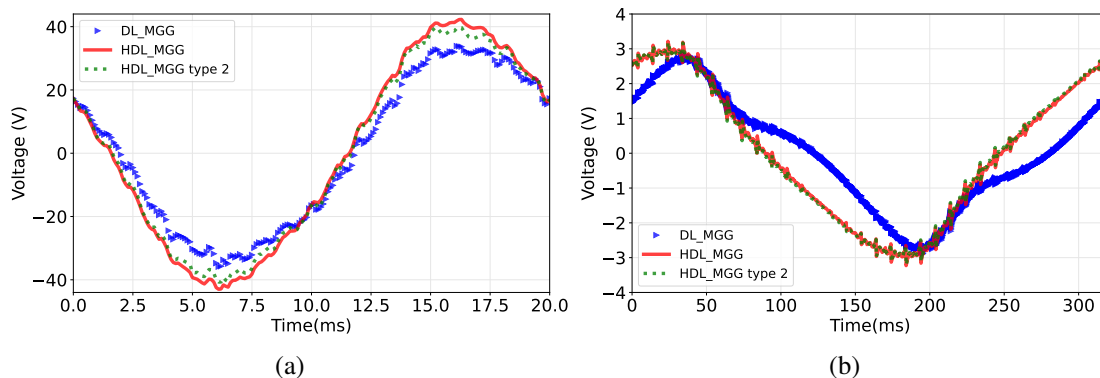(a)   (b)

Figure 15. Voltages of (a) inner and (b) outer stator back-EMF waveform

Table 2. Magnetic geared generator structures outputs

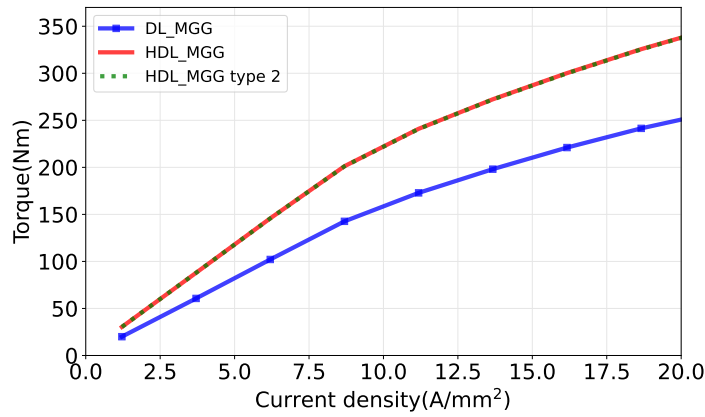| Parameters | Magnetic geared generator structures | | | | | |
| | Inner Stator | | | Outer Stator | | |
	DL-MGG	HDL-MGG	HDL-MGG type2	DL-MGG	HDL-MGG	HDL-MGG type2
Max voltage (V)	36.01	43.269	41.614	2.883	3.236	3.201
Max current (A)	9	9	9	8.2	7.7	7.5
Power factor	0.851	0.909	0.903	0.929	0.996	0.988

Figure 16. The torque of the coil voltage versus the current of the outer stator excitation

6. VARIABLE-SPEED CONSTANT-FREQUENCY PERFORMANCE

As shown in Figure 17, in the proposed system in the dual-rotor wind turbine, by changing the inner rotor speed from 127.6 rpm to 196 rpm due to fluctuation in wind speed, the outer rotor speed has to change from 10 rpm to 100 rpm. Figure 18 illustrated that the frequency of the outer stator current and voltage changes from 3.167 Hz to 31.67 Hz. It is shown in Figure 19 that the frequency of the current and voltage of the inner stator remains constant. Therefore, these configurations validate variable-speed constant-frequency.
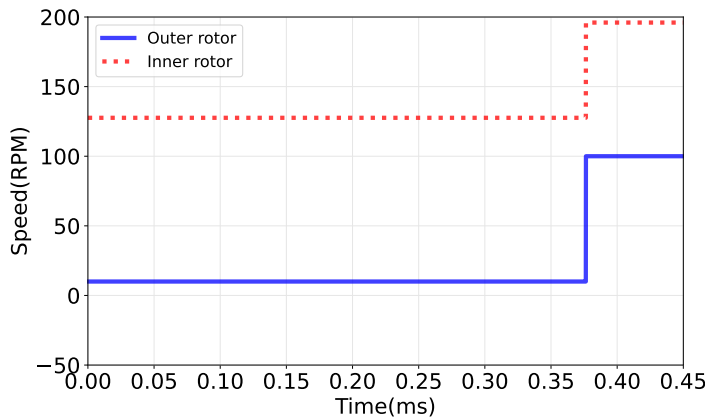
Figure 17. Variation speed of the inner and outer rotor

| Outer stator winding current | Outer stator winding voltage |
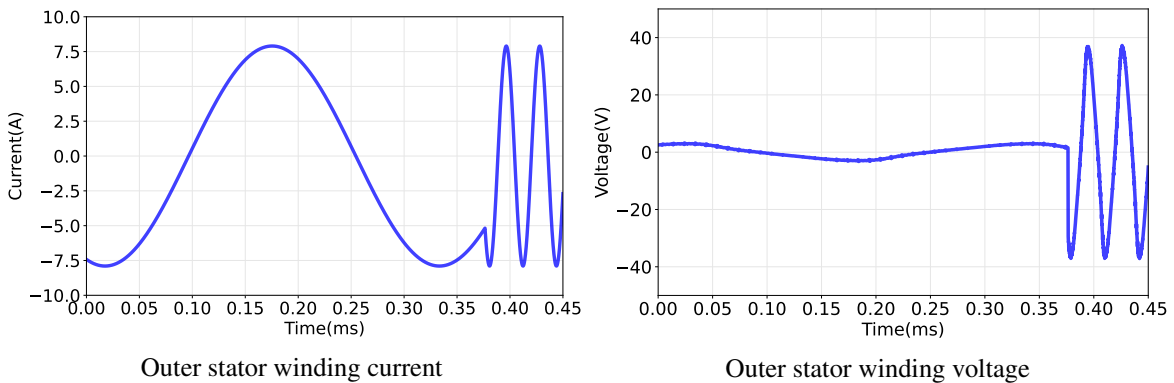
Figure 18. Variable-speed constant-frequency performance of outer stator winding current and voltage

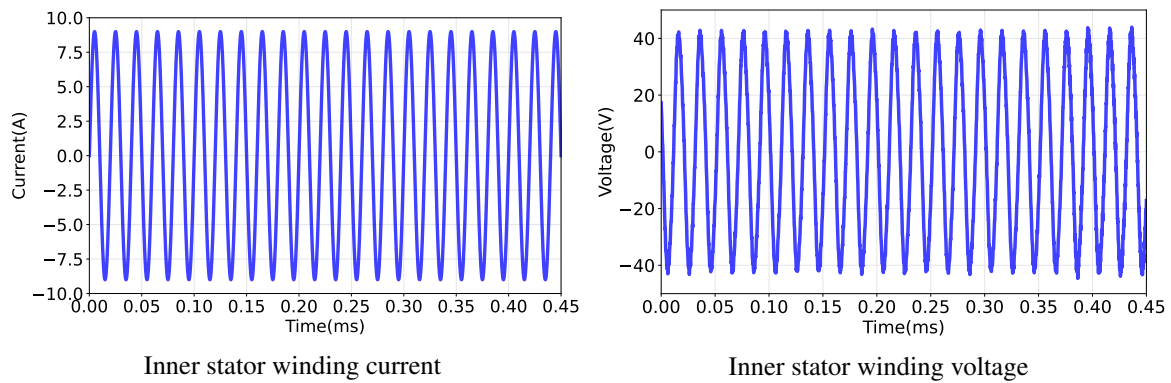| Inner stator winding current | Inner stator winding voltage |

Figure 19. Variable-speed constant-frequency performance of inner stator winding current and voltage

7. CONCLUSIONS

The utilization of variable-speed constant-frequency generating systems can significantly enhance the efficiency of wind power. However, previous structures have been limited by their low torque density. Therefore, this study presents a novel magnetic geared generator structure designed to improve both torque density and power factor. Additionally, this innovative structure is employed in conjunction with a dual-rotor wind turbine to increase the captured input power by utilizing two wind rotors. In this configuration, the outer rotor serves as a control rotor, eliminating the need for a high-power converter for output power and instead benefiting from a low-power converter to control the system, which constitutes the first novelty of this approach. The proposed structure is suitable for applications in wind turbines and electric vehicles, enabling precise control of rotor velocity. It offers a potential alternative to traditional gear and generator systems employed in wind turbines. It is important to note that the presence of different magnetization directions poses a challenge in implementing this structure, potentially increasing implementation costs. However, the higher power factor provided by this novel proposed structure presents an important reason to invest in this novel structure. The main drawback of this proposed structure is its complex design, which raises the total cost. Future research will focus on including different magnet configurations, like the bread loaf shaped magnet and sinusoidal plus third harmonic shaped magnets.

REFERENCES

[1] H. Polinder, J. A. Ferreira, B. B. Jensen, A. B. Abrahamsen, K. Atallah, and R. A. McMahon, "Trends in wind turbine generator systems," *IEEE Journal of Emerging and Selected Topics in Power Electronics*, vol. 1, no. 3, pp. 174–185, 2013, doi: 10.1109/JESTPE.2013.2280428.

[2] E. Taherian-Fard, R. Sahebi, T. Niknam, A. Izadian, and M. Shasadeghi, "Wind turbine drivetrain technologies," *IEEE Transactions on Industry Applications*, vol. 56, no. 2, pp. 1729–1741, 2020, doi: 10.1109/TIA.2020.2966169.

[3] K. Arthishri, N. Kumaresan, and N. A. Gounden, "Analysis and application of three-phase SEIG with power converters for supplying single-phase grid from wind energy," *IEEE Systems Journal*, vol. 13, no. 2, pp. 1813–1822, 2019, doi: 10.1109/JSYST.2018.2875761.

[4] H. Benbouhenni, "Application of DPC and DPC-GA to the dual-rotor wind turbine system with DFIG," *IAES International Journal of Robotics and Automation (IJRA)*, vol. 10, no. 3, 2021, doi: 10.11591/ijra.v10i3.pp224-234.

[5] L. Shao, W. Hua, J. Soulard, Z. Q. Zhu, Z. Wu, and M. Cheng, "Electromagnetic performance comparison between 12-phase switched flux and surface-mounted pm machines for direct-drive wind power generation," *IEEE Transactions on Industry Applications*, vol. 56, no. 2, pp. 1408–1422, 2020, doi: 10.1109/TIA.2020.2964527.

[6] K. Li, S. Modaresahmadi, W. B. Williams, J. Z. Bird, J. D. Wright, and D. Barnett, "Electromagnetic analysis and experimental testing of a flux focusing wind turbine magnetic gearbox," *IEEE Transactions on Energy Conversion*, vol. 34, no. 3, pp. 1512–1521, 2019, doi: 10.1109/TEC.2019.2911966.

[7] O. Dobzhanskyi *et al.*, "Axial-flux PM disk generator with magnetic gear for oceanic wave energy harvesting," *IEEE Access*, vol. 7, pp. 44813–44822, 2019, doi: 10.1109/ACCESS.2019.2908348.

[8]   F. K. Moghadam and A. R. Nejad, "Evaluation of PMSG-based drivetrain technologies for 10-MW floating offshore wind turbines: pros and cons in a life cycle perspective," *Wind Energy*, vol. 23, no. 7, pp. 1542–1563, 2020, doi: 10.1002/we.2499.

[9]   L. Jian, K. T. Chau, and J. Z. Jiang, "A magnetic-geared outer-rotor permanent-magnet brushless machine for wind power generation," *IEEE Transactions on Industry Applications*, vol. 45, no. 3, pp. 954–962, 2009, doi: 10.1109/TIA.2009.2018974.

[10]   D. Gielen, *Renewable energy technology cost analysis series*, IRENA, European Union, 2012.

[11]   P. Alotto *et al.*, "Design, analysis and realisation of a magnetic gear prototype with experimental validation," in *2022 23/textsuperscriptrd International Conference on the Computation of Electromagnetic Fields (COMPUMAG)*, Jan. 2022, pp. 1–4, doi: 10.1109/COMPUMAG55718.2022.9827514.

[12]   K. Atallah, S. D. Calverley, and D. Howe, "Design, analysis and realisation of a high-performance magnetic gear," *IEE Proceedings: Electric Power Applications*, vol. 151, no. 2, pp. 135–143, 2004, doi: 10.1049/ip-epa:20040224.

[13]   P. M. Tlali, R. J. Wang, S. Gerber, C. D. Botha, and M. J. Kamper, "Design and performance comparison of vernier and conventional PM synchronous wind generators," *IEEE Transactions on Industry Applications*, vol. 56, no. 3, pp. 2570–2579, 2020, doi: 10.1109/TIA.2020.2979111.

[14]   J. Zhang, Y. Jiang, X. Hu, and S. Xu, "A brushless doubly fed generator based on permanent magnet field modulation," *IEEE Transactions on Industrial Electronics*, vol. 67, no. 5, pp. 3505–3516, 2020, doi: 10.1109/TIE.2019.2916381.

[15]   S. Niu, S. L. Ho, and W. N. Fu, "A novel double-stator double-rotor brushless electrical continuously variable transmission system," *IEEE Transactions on Magnetics*, vol. 49, no. 7, pp. 3909–3912, 2013, doi: 10.1109/TMAG.2013.2248347.

[16]   Y. Wang, S. Niu, W. N. Fu, and S. L. Ho, "Design and optimization of electric continuous variable transmission system for wind power generation," *IEEE Transactions on Magnetics*, vol. 52, no. 3, pp. 1–4, 2016, doi: 10.1109/TMAG.2015.2487995.

[17]   H. Zhao, C. Liu, Z. Song, and S. Liu, "A consequent-pole PM magnetic-geared double-rotor machine with flux-weakening ability for hybrid electric vehicle application," *IEEE Transactions on Magnetics*, vol. 55, no. 7, pp. 1–7, 2019, doi: 10.1109/TMAG.2019.2901265.

[18]   Y. Mao, S. Niu, and Y. Yang, "Differential evolution-based multiobjective optimization of the electrical continuously variable transmission system," *IEEE Transactions on Industrial Electronics*, vol. 65, no. 3, pp. 2080–2089, 2018, doi: 10.1109/TIE.2017.2733458.

[19]   E. Erturk, S. Sivrioglu, and F. C. Bolat, "Analysis model of a small scale counter-rotating dual rotor wind turbine with double rotational generator armature," *International Journal of Renewable Energy Research*, vol. 8, no. 4, pp. 1849–1858, 2018, doi: 10.20508/ijrer.v8i4.8235.g7549.

[20]   L. Romański, J. Bieniek, P. Komarnicki, M. Debowski, and J. Detyna, "Operational tests of a dual-rotor mini wind turbine," *Eksploatacja i Niezawodnosc*, vol. 18, no. 2, pp. 201–209, 2016, doi: 10.17531/ein.2016.2.7.

[21]   E. M. Farahani, N. Hosseinzadeh, and M. M. Ektesabi, "SSR risk alleviation in dual-rotor wind turbine by employing genetic solutions," 2011.

[22]   R. W. Y. Habash, V. Groza, and P. Guillemette, "Performance optimization of a dual-rotor wind turbine system," in *2010 IEEE Electrical Power and Energy Conference*, Aug. 2010, pp. 1–6, doi: 10.1109/EPEC.2010.5697229.

[23]   E. M. Farahani, N. Hosseinzadeh, and M. E. Mehran, "Comparison of dynamic responses of dual and single rotor wind turbines under transient conditions," in *2010 IEEE International Conference on Sustainable Energy Technologies (ICSET)*, Dec. 2010, pp. 1–8, doi: 10.1109/ICSET.2010.5684946.

[24]   X. Luo and S. Niu, "A novel contra-rotating power split transmission system for wind power generation and its dual MPPT control strategy," *IEEE Transactions on Power Electronics*, vol. 32, no. 9, pp. 6924–6935, 2017, doi: 10.1109/TPEL.2016.2629021.

[25]   A. Rosenberg, S. Selvaraj, and A. Sharma, "A novel dual-rotor turbine for increased wind energy capture," in *Journal of Physics: Conference Series*, 2014, vol. 524, no. 1, doi: 10.1088/1742-6596/524/1/012078.

[26]   S. Niu, S. L. Ho, and W. N. Fu, "Design of a novel electrical continuously variable transmission system based on harmonic spectra analysis of magnetic field," *IEEE Transactions on Magnetics*, vol. 49, no. 5, pp. 2161–2164, 2013, doi: 10.1109/tmag.2013.2243116.

[27]   Q. Ma, A. El-Refaie, and B. Lequesne, "Low-cost interior permanent magnet machine with multiple magnet types," *IEEE Transactions on Industry Applications*, vol. 56, no. 2, pp. 1452–1463, 2020, doi: 10.1109/TIA.2020.2966458.

[28]   S. Yousefnejad, H. Heydari, K. Akatsu, and J. S. Ro, "Analysis and design of novel structured high torque density magnetic-geared permanent magnet machine," *IEEE Access*, vol. 9, pp. 64574–64586, 2021, doi: 10.1109/ACCESS.2021.3076260.

[29]   S. Niu, T. Sheng, X. Zhao, and X. Zhang, "Operation principle and torque component quantification of short-pitched flux-bidirectional-modulation machine," *IEEE Access*, vol. 7, pp. 136676–136685, 2019, doi: 10.1109/ACCESS.2019.2942482.

[30]   Y. Zheng, L. Wu, J. Zhu, Y. Fang, and L. Qiu, "Analysis of dual-armature flux reversal permanent magnet machines with Halbach array magnets," *IEEE Transactions on Energy Conversion*, vol. 36, no. 4, pp. 3044–3052, 2021, doi: 10.1109/TEC.2021.3070039.

[31]   Z. Song, C. Liu, and H. Zhao, "Investigation on magnetic force of a flux-modulated double-rotor permanent magnet synchronous machine for hybrid electric vehicle," *IEEE Transactions on Transportation Electrification*, vol. 5, no. 4, pp. 1383–1394, 2019, doi: 10.1109/TTE.2019.2946494.

[32]   X. Zhu, C. H. T. Lee, C. C. Chan, L. Xu, and W. Zhao, "Overview of flux-modulation machines based on flux-modulation principle: topology, theory, and development prospects," *IEEE Transactions on Transportation Electrification*, vol. 6, no. 2, pp. 612–624, 2020, doi: 10.1109/TTE.2020.2981899.

[33]   M. Filippini *et al.*, "Magnetic loss analysis in coaxial magnetic gears," *Electronics*, vol. 8, no. 11, Nov. 2019, doi: 10.3390/electronics8111320.

[34]   T. S. No, J. E. Kim, J. H. Moon, and S. J. Kim, "Modeling, control, and simulation of dual rotor wind turbine generator system," *Renewable Energy*, vol. 34, no. 10, pp. 2124–2132, 2009, doi: 10.1016/j.renene.2009.01.019.

[35]   S. Yousefnejad and E. Amiri, "Consequent-pole dual-layer axial flux magnetic gear with Halbach array," in *2023 IEEE International Electric Machines and Drives Conference (IEMDC)*, May 2023, pp. 1–5, doi: 10.1109/IEMDC55163.2023.10239032.

[36]   X. Liu, Y. Zhao, Z. Chen, D. Luo, and S. Huang, "Multi-objective robust optimization for a dual-flux-modulator coaxial magnetic gear," *IEEE Transactions on Magnetics*, vol. 55, no. 7, pp. 1–8, 2019, doi: 10.1109/TMAG.2018.2887273.

[37]   L. Jian and K. T. Chau, "A coaxial magnetic gear with Halbach permanent-magnet arrays," *IEEE Transactions on Energy Conversion*, vol. 25, no. 2, pp. 319–328, 2010, doi: 10.1109/TEC.2010.2046997.

[38]   S. Yousefnejad, H. Heidary, J.-S. Ro, E. Amiri, S. Ebrahim Afjei, and K. Akatsu, "A novel structure of magnetic-geared permanent

magnet machine based on Halbach array," in *2022 IEEE Kansas Power and Energy Conference (KPEC)*, Apr. 2022, pp. 1–6, doi: 10.1109/KPEC54747.2022.9814759.

[39] S. Teymoori, A. Rahideh, H. Moayed-Jahromi, and M. Mardaneh, "2-D analytical magnetic field prediction for consequent-pole permanent magnet synchronous machines," *IEEE Transactions on Magnetics*, vol. 52, no. 6, pp. 1–14, 2016, doi: 10.1109/TMAG.2016.2521834.

[40] Y. Wang, S. Niu, and W. Fu, "Sensitivity analysis and optimal design of a dual mechanical port bidirectional flux-modulated machine," *IEEE Transactions on Industrial Electronics*, vol. 65, no. 1, pp. 211–220, 2018, doi: 10.1109/TIE.2017.2719620.

[41] Q. Wang, S. Niu, and S. Yang, "Design optimization and comparative study of novel magnetic-geared permanent magnet machines," *IEEE Transactions on Magnetics*, vol. 53, no. 6, pp. 1–4, 2017, doi: 10.1109/tmag.2017.2662947.

[42] S. S. Mustafa, N. Misron, N. Mariun, M. L. Othman, and T. Hanamoto, "Torque distribution characteristics of a novel double-stator permanent magnet generator integrated with a magnetic gear," *Energies*, vol. 10, no. 1, 2017, doi: 10.3390/en10010002.

BIOGRAPHIES OF AUTHORS

Soheil Yousefnejad ⓘ 🕮 sᴄ ↻ received a B.S. degree in electrical engineering from Shahid Beheshti University, Tehran, Iran, in 2015, and an M.Sc. degree from the Iran University of Science and Technology (IUST), Tehran, in 2018, both in electrical power engineering. He is currently pursuing a Ph.D. degree in electrical engineering at the University of New Orleans, New Orleans, LA, USA. His research interests include magnetic gears, electrical machine design, and lithium-ion battery chargers. He can be contacted at syousefn@my.uno.edu.

Hossein Heydari ⓘ 🕮 sᴄ ↻ received a B.S. degree in electrical engineering and an M.Sc. degree in power electronics from Loughborough University, Loughborough, U.K. in 1985 and 1987, respectively, and a Ph.D. degree in transformer core losses from the University of Wales, Cardiff, U.K. in 1993. Following graduation, he joined the Iran University of Science and Technology (IUST), Tehran, Iran, as an academic member (lecturer) of the Electrical Power Group and was also appointed as Director of the High Voltage and Magnetic Materials Research Center. He is currently with the Center of Excellence for Power System Automation and Operation, IUST. His research interests are EMC considerations in power systems, magnetic gears, fault current limiters, and applied superconductivity in power systems. He can be contacted at heydari@iust.ac.ir.

Vincenzo Cirimele ⓘ 🕮 sᴄ ↻ (Member, IEEE) was born in Verbicaro, Italy, in 1987. He received an M.Sc. degree in electrical engineering from the Politecnico di Torino, Turin, Italy and a Ph.D. degree in electronic engineering and electrical engineering from the Politecnico di Torino and Université Paris-Saclay, Paris, France, in February 2017. He is currently an assistant professor with the Department of Energy, Politecnico di Torino. His research interests include the protection of people from the magnetic field at industrial frequency, electromagnetic modeling, and inductive power transmission for electric vehicles. He can be contacted at vincenzo.cirimele@unibo.it.

Jong-Suk Ro ⓘ 🕮 sᴄ ↻ received his Ph.D. in Electrical Engineering from the Seoul National University, Seoul, Korea, in 2008 and his B.S. degree in Mechanical Engineering from the Han-Yang University, Seoul, Korea, in 2001. Currently, he is a full professor at the School of Electrical and Electronics Engineering and an adjunct professor at the Department of Intelligent Energy and Industry, Chung-Ang University, Seoul, Korea. In 2014, he was with the University of BATH, Bath, as UK an Academic Visitor. From 2013 to 2016, he worked with Brain Korea 21 Plus, Seoul National University, as a BK Assistant Professor. He conducted research at the Electrical Energy Conversion System Research Division of the Korea Electrical Engineering & Science Research Institute as a researcher in 2013. From 2012 to 2013, he was with the Brain Korea 21 Information Technology of Seoul National University, as a post-doctoral fellow. He conducted research at the R&D center of Samsung Electronics as a Senior Engineer from 2008 to 2012. His research interests include the analysis and optimal design of electric machines. He can be contacted at jongsukro@gmail.com.